Measurement 220 (2023) 113404

Contents lists available at ScienceDirect

Measurement

journal homepage: www.elsevier.com/locate/measurement

Grid-layout ultrasonic LoRaWAN-based sensor networks for the measurement of the volume of granular materials

Alessandro Pozzebon [a,*], Marco Benini [b], Cristiano Bocci [b], Ada Fort [b], Stefano Parrino [b], Fabio Rapallo [c]

[a] Department of Information Engineering, University of Padova, Via Gradenigo 6/b, 35131 Padova, Italy
[b] Department of Information Engineering and Mathematics, University of Siena, Via Roma 56, 53100 Siena, Italy
[c] Department of Economics, University of Genova, Via Vivaldi 5, 16126 Genova, Italy

ARTICLE INFO

Keywords:
Granular materials
Volume measurement
Ultrasonic sensors
Grid-layout networks
Geometry

ABSTRACT

The aim of this paper is to propose a novel methodology for the measurement of volume of masses of granular material: this term encompasses a wide range of materials like grain, sand, coal and so on. The proposed approach is based on the exploitation of grids of ultrasonic ranging sensor nodes, placed above the material mass, exploiting LoRaWAN connectivity for data transmission and measuring the actual level of the material in each single spot. A geometrical approach is applied to the measured data for the computation of the volume. The proposed approach was tested by means of simulations and exploiting a reduced-scale experimental setup: different grid layouts were implemented and tested, with the aim of increasing the measurement accuracy. Since the presented experimental setup can be seen as a worst case scenario, the achieved results can be assumed as an upper bound for the accuracy of the proposed layout.

1. Introduction

The term "Granular Materials", or "Bulk Solids", is used to indicate all those materials which are composed of individual solid particles whose size does not allow them to be subject to thermal motion fluctuations: this happens when the diameter of the single particles composing the solid is in the [0.1 μm, 10 mm] range [1]. Such definition encompasses a huge number of materials which are massively present in nature and extensively treated in industrial processes [2]: the most common example of a granular material is sand, but countless, heterogeneous examples can be cited, like grain, coal, rice, snow, pills and so on.

The peculiar features of these materials pose them halfway between solids and liquids: in particular, their distribution changes according to movements of the single particles or swarm of particles, similarly as liquids, but they do not fully assume the shape of the container in which they are placed, a typical feature of liquids. This means that a mass of granular materials does not have a flat surface: the shape of the surface is in general due to a large number of different phenomena. As an example we may think of sand, whose superficial shape is due to a large number of physical and meteorological phenomena (wind, erosion, water, rain, etc.) or to grain in a granary: in this case, the shape of the upper surface is mainly due to the way grain is inserted inside the structure (from a central or a lateral opening).

Such features make the measurement of the volume of any kind of granular material by far more challenging than in the case of solids or liquids. Indeed, the volume of a solid is not subject to change: however, in case of change, it can easily be estimated by acquiring the weight of the solid itself once its density is known. A number of papers focusing on solids can be found in literature, in general exploiting imaging [3–7]. Regarding liquids, their volume can be estimated again by measuring the weight if the density is known. When liquids are stored in containers, an alternative way to measure their volume is by measuring the empty volume of tanks and containers [8,9] or by acquiring the level of the liquid itself inside the container [10–15]. This can be done exploiting a large number of sensors: these include for example ultrasonic [16], capacitive [17] or fiber optic [18] sensors.

Conversely, the case of granular material is by far more complex since the shape of the material as well as the way it is distributed in each specific container have to be taken into account. Moreover, its value is subject to continuous changes due to movements of the particles: as a matter of fact, a local measurement of the material level or the measurement of its weight is thus not sufficient to allow an estimation of the overall volume. For this reason, other techniques have to be evaluated, taking into account also the measurement system requirements related to the deployment site. These may foresee the

* Corresponding author.
E-mail address: alessandro.pozzebon@unipd.it (A. Pozzebon).

https://doi.org/10.1016/j.measurement.2023.113404
Received 2 February 2023; Received in revised form 4 July 2023; Accepted 30 July 2023
Available online 4 August 2023

usage of complex sensors and devices like cameras [19] or Unmanned Aerial Vehicles (UAVs) [20–22], or may require the integration of a larger number of sensor nodes [23] like the solution presented in this paper, possibly keeping low their overall cost in order to foster its adoption in large numbers. In line with this approach, this paper proposes a technological infrastructure based on low cost ultrasonic sensors, arranged according to a grid-layout, able to remotely transmit the collected data thanks to the Long Range (LoRa) transmission technology together with the LoRa Wide Area Network (LoRaWAN) protocol. Thanks to the low cost of the sensors, different layouts can be envisaged, in order to increase the overall accuracy of the volume estimation.

While this approach is novel and to our knowledge has never been presented, a number of works dealing with granular materials can be found in literature. Some of them are not directly targeted towards the actual measurement of the volume but only of the surface level, having in general silos as main targets. Indeed, these structures have a diameter which is by far smaller than their height: this means that through a single measurement of the level, the volume can be easily assessed with an acceptable accuracy. An interesting overview of the techniques that can be applied to the measurement of the level of bulk solids stored in silos is provided in [24], while a detailed architecture proposing the usage of three capacitive sensors is described in [25].

The idea of exploiting information about the level for the estimation of the granular material volume with a higher accuracy is presented in [26], where radar is employed to reconstruct the upper surface of the grain stored in a silos, and then to calculate the volume according to a geometrical approach presented in [27]. The approach presented in [26] is further extended in [28], where machine learning techniques are applied for the grain quantity estimation. A similar approach is presented in [29], where UAVs are used to estimate the upper surface of a load of sand stored in a sand carrier. Following the laser scanning of the surface, the volume is obtained by resorting to the dimensions of the carrier, which are a priori known. At a larger scale, satellite images, photogrammetry and lidar have been extensively used to estimate the material volume in large areas, for example in sand dunes [30,31] or sand quarries [32]. However, while these approaches may be in some way similar to the one presented in this paper, the required instrumentation is by far more expensive. Moreover, the usage of the AUV does not allow for a continuous real time monitoring: these requirements are not mandatory for the specific application (the load in the carrier is expected not to change with time) but may be crucial in other application scenarios. Similarly, Turner et at. [33] propose the estimation of bulk solids volume in silos exploiting low density point clouds acquired by means of a laser distance meter: again, this solution is based on expensive devices and complex computing techniques, and does not foresee real time and continuous data acquisition.

A limited number of works focuses specifically on the volume estimation of piles of bulk material. Their approaches are the most similar to the experimental setup presented in this paper and different techniques are employed for the estimation. The solution presented in [34] exploits Microsoft Kinect to estimate the actual shape of heaps of a number of different materials (e.g., lignite, wood chips, coke, etc...): while this work does not focus directly on volume measurement, this latter is obtained in the preliminary phase of the technique presented in this paper, where the shape of the upper surface of the bulk material is estimated by means of sensed data. Actual volume measurements exploiting imaging are presented in [35] by means of range imaging (RIM) camera and in [36] using laser telemeters on piles of coal, while Yanling et al. [37] propose a technique based on reverse engineering, exploiting point clouds to achieve a 3D polygonal model of the upper surface of the material.

A solution based on ultrasonic ranging was only devised in one contribution: in [38], an array of ultrasonic sensors was employed to acquire the profiles of a mass of bulk material. However, the system was only tested on an empty box of known volume, proposing a different computation approach deriving from the deployment of the sensor array on a conveyor belt. Accordingly, the solution proposed in this work has never been presented in the literature for what concerns both the measurement system architecture and the computation process.

The rest of the paper is structured as follows: Section 2 presents the approach proposed in this paper and the architecture of the technological infrastructure, while the algorithm adopted for the calculation of the volume is described in Section 3. Section 4 describes the different layouts of the distributed measurement system, while simulations are presented in Section 5. The experimental setup and the field tests are presented respectively in Sections 6 and 7. Test results are then discussed in Section 8 while Section 9 presents some conclusive remarks.

2. System architecture

The proposed system aims at measuring the volume of granular materials by means of a sensor network: in such architecture, sensors are positioned according to a specific space arrangement, being in charge of measuring the level of the material in a set of specific points. In the simplest case, one sensor is placed at each corner of a square delimiting the measurement area. However, different layouts can be envisaged: in particular, in Section 4 new configurations will be proposed, suggesting the usage of more than one sensor for a sub-set of the measurement spots, with the aim of increasing the overall accuracy and reliability of the measurement system.

Regarding the measurement technique for the material level, as explained in [39], such task can be accomplished exploiting three sensing strategies. Indeed, sensors can be positioned on the floor of the deployment site (i.e., below the granular material): in this case, weight sensors (for example, piezoelectric sensors) can be used to estimate the weight of the material in each specific point and thus extract the actual material level. Another option foresees the positioning of poles in charge of detecting the level of the material by measuring the height of the buried section of the pole itself. Both these solutions are suitable to be employed outdoor, where the granular material is not provided with any type of coverage.

The last option, and the one adopted in this work, is designed for those situations where the material is stored indoor or under any type of coverage: in this case, sensors can be deployed above the surface of the granular material, e.g. fixed to the coverage, and the level of the material is then estimated by measuring the distance of the material surface from the fixed sensor positions. Such a solution can be easily employed in a number of application scenarios, for example in case of warehouses, granaries or any other indoor storage site. In this case a distance measurement is exploited, therefore a wide range of sensor typologies can be used: one good option is represented by ultrasonic ranging sensors, which have very low costs, limited power consumption, and are able to work in a wide range of operating conditions with obvious advantages with respect to other technologies (e.g. infrared sensors). While these sensors are only able to measure the distance of the material surface from the coverage on which they are fixed, the actual material thickness can be indirectly measured by knowing the exact positioning height of the sensors: by subtracting the measured distance from this value, the thickness value is achieved.

The architecture presented and tested in this paper is shown in Fig. 1 and is based on a set of sensor nodes integrating ultrasonic sensors, provided with long range wireless connectivity, and battery-powered, adopting however power reduction policies to improve the lifetime of the devices. Regarding the connectivity, different choices could be made, exploiting either local or wide area technologies. Local area technologies are ideal when reduced power consumption is required and the area to be covered has a range below 100 m: in this case, Bluetooth is probably the best option. In particular, Bluetooth 5 modules require a very limited amount of power to transmit (in general in the order of 10 mW) and their cost is in the order of few of euros: as an example, BM70/71 modules by Microchip have a declared

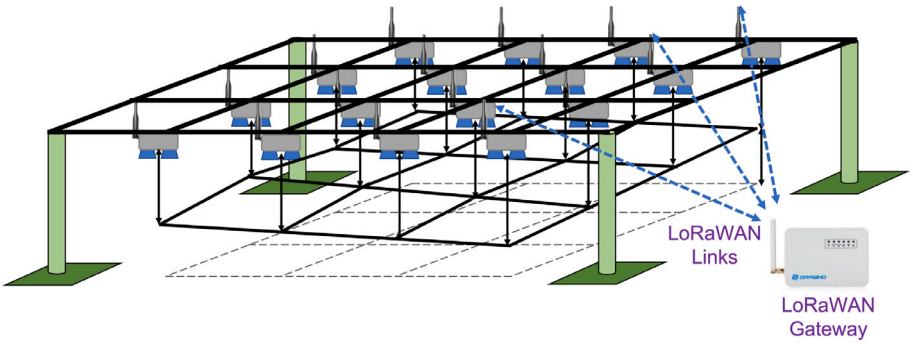

Fig. 1. System Architecture.

current absorption in transmission of 3.3 mA at 3.0 V (and thus a 10 mW power consumption) [40]. While such features may suggest to choose this option, local area technologies have the drawback of requiring a local gateway: this means that a more complex network infrastructure is required when large areas have to be covered. Long range solutions allow to overcome this problem, however at a price of higher power consumption. Nevertheless, a number of technologies has emerged in the last 10 years, allowing the implementation of long range communication, while keeping low the amount of required power. Among these technologies, LoRa is probably the one that has seen the largest development and adoption at a global level.

LoRa operates in the unlicensed Industrial, Scientific and Medical (ISM) bands of 433, 868 and 915 MHz and it is based on the proprietary Chirp Spread Spectrum (CSS) modulation, patented by Semtech [41]: this is a frequency modulation where symbols are encoded in chirps, i.e., sinusoidal signals whose frequency is modulated with linear sweeps, increasing (up-chirp) or decreasing (down-chirp) over time. Such modulation allows to achieve receiver sensitivity values up to −146 dB, which entail transmission distances up to some tens of kms outdoors in rural areas. These performances are scaled in indoor environments: however, with a single gateway it is still possible to cover large scale buildings, with a notable reduction in complexity with respect to local area technologies which require the deployment of large quantities of access points. LoRa performances in terms of transmission ranges and power consumption can be partially customized by modifying a set of transmission parameters: these include the Spreading Factor (SF), the Bandwidth (BW) and the Coding Rate (CR). The SF ranges from 7 to 12 and affects the speed of the chirps: a higher SF entails a higher power consumption but also a larger transmission distance. The BW is basically the spectral width of the chirp: three values are allowed (125 kHz, 250 kHz and 500 kHz) and a smaller BW allows to reach larger transmission distances while a larger value reduces the Time on Air (ToA) and thus the power consumption. Finally, the CR indicates the number of redundant bits for Forward Error Correction (FEC): 4 values are allowed (4/5, 4/6, 4/7 and 4/8) and a lower value implies longer ToA but also a higher chance to correctly demodulate the packets. All these values can be customized according to each specific application requirement: for this reason, in this work the adoption of LoRa was preferred with respect to local area technologies like Bluetooth or WiFi. As already stated, even if LoRa requires a larger amount of power with respect to Bluetooth, such value is still acceptable for long term monitoring. Moreover, LoRa demonstrated to be immune to interference and heavy multi-path for higher SF values [42]. Similarly, LoRa modulation proven to be robust also to possible interferences caused by competing technologies in the same ISM bands, like SigFox, Z-Wave or IO Home Control [43]. Finally, LoRa packet collisions proven to be critical only in case of the same SF and of transmissions on the same channel, remembering that LoRa transmissions can exploit 8 different channels [44].

LoRa is complemented by the LoRaWAN protocol, which implements policies devoted to power consumption reduction like Adaptive Data Rate (ADR), an adaptive setting of the aforementioned LoRa radio parameters according to the best ratio between low power consumption and successful transmission. LoRaWAN foresees a star network topology where end nodes transmit packets to one or more gateways which are in charge of forwarding them to the server structure: this is composed of a Network Server, in charge of managing all the incoming packets, and an Application Server, which is in charge of processing the data. The only limitation that has to be taken into account in any LoRaWAN transmission is related to the duty-cycle: indeed, according to the local regulations, in most countries this limit is set to 1% [45]. This means that a significant time has to be waited between one transmission and the following: however, this is not an issue for the proposed application since granular material volume measurements are not expected to be performed frequently. As a positive side effect, such regulation notably reduces the chance of packet collisions.

The general architecture of each of the sensor nodes presented in this paper integrates one or more ultrasonic ranging sensors according to the specific network layout, a microcontroller for data acquisition and processing, a LoRa module and the batteries. The ultrasonic sensor is the HC-SR04, produced by a number of manufacturers and featuring a detection range from 2 cm to 400 cm, with a declared accuracy of 0.3 cm. However, such value appears to be underestimated and for the current application, due to the contribution of the front-end electronics for the Time of Flight estimation, an accuracy of ±1 cm was assessed. The HC-SR04 sensor operates at the frequency of 40 kHz, and has separate emitter and receiver: this allows to obtain a relatively narrow angle of 15°. Such feature is crucial in punctual distance measurements since larger angles do not provide a sufficient spatial resolution. Together with these features, this sensor was also chosen for its low cost, which is in the order of few euros. The microcontroller performing data acquisition and processing is an ATtiny861A by Atmel/Microchip: this device was chosen since the system has to perform a very limited number of operations, but the power consumption is crucial. The current absorption of the ATtiny861A is 200 μA for 1.8 V powering voltage when operating at 1 MHz clock frequency: such value drops down to 2 μA if the microcontroller is put in power-down mode [46].

Data transmission is performed by means of an RFM95 LoRa module by HopeRF, connected to the microcontroller by means of Serial Peripheral Interface (SPI) protocol. The network infrastructure is set up exploiting an LG308 Dragino gateway in charge of forwarding the received packets to the LoRaWAN Network and Application Servers by means of WiFi connectivity.

Finally, the node is powered by means of two 3.7 V 18650 Li-Ion batteries featuring large capacity (up to 6800 mAh), required since the HC-SR04 sensor needs a supply voltage of 5 V.

3. Algorithm for volume estimation

In [39] we proposed a mathematical model for the calculation of the volume of granular masses. In that case we considered a three-dimensional shape $F \subset \mathbb{R}^3$, given by a rectangular parallelepiped, with

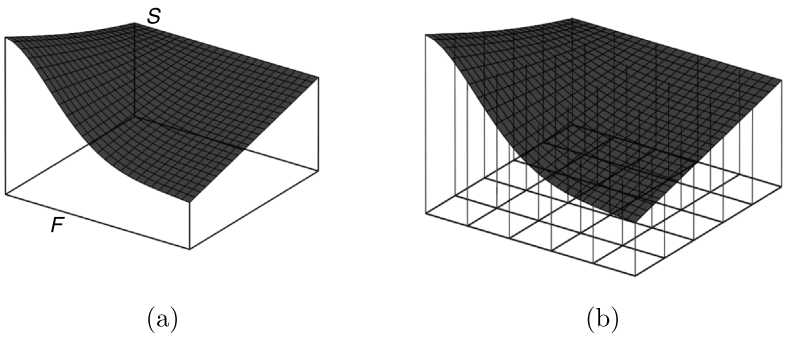

Fig. 2. Example of regular surface (a) and corresponding Base sensor layout (b).

square base of edge l, but upperly limited by a regular surface S as in Fig. 2(a). We can assume that the base of F lies in the plane $z = 0$ and hence the vertex points of the base have coordinates $(0,0)$, $(l,0)$, $(0,l)$ and (l,l).

The approximation of the volume of F was given by considering a grid of $(n+1)\times(n+1)$ points in the base, with coordinates $(i\frac{l}{n}, j\frac{l}{n}, 0)$ for $0 \le i,j \le n$. Fig. 2(b) shows the case in which $n = 5$. Let a_{ij} be the height of F in correspondence of the points of the grid $(i\frac{l}{n}, j\frac{l}{n}, 0)$, that is we know the points $(i\frac{l}{n}, j\frac{l}{n}, a_{ij})$, where the $a_{i,j}$ are the measurements of the sensors. The approximated volume of F will be given by the sum of the average volumes of the triangular subdivisions of each block of the grid. Notice that in this case the area of each triangular base is $A = \frac{l^2}{2n^2}$. Hence, the volume can be approximated by the following:

$$V_{approx} = \frac{l^2}{4n^2} \cdot \sum_{i,j=0}^{n-1} (a_{i,j} + a_{i,j+1} + a_{i+1,j} + a_{i+1,j+1}), \tag{1}$$

which can be rewritten as

$$\begin{aligned} V_{approx} = {} & \frac{l^2}{4n^2} \cdot \left(a_{0,0} + a_{0,n} + a_{n,0} + a_{n,n}\right) + \\ & + \frac{l^2}{2n^2} \cdot \sum_{i=1}^{n-1} (a_{0,i} + a_{l,i} + a_{i,0} + a_{i,l}) + \\ & + \frac{l^2}{n^2} \cdot \sum_{i,j=1}^{n-1} a_{i,j}. \end{aligned} \tag{2}$$

From now, we refer to the model introduced in [39] as "Base model".

4. Grid configurations

The model in Eq. (2) was described and characterized in a previous work by the authors [39]. In that work, a set of simulations was used to assess the model performance in terms of accuracy, but that setup assumed the usage of LDR sensor arrays. The resolution of the LDR sensors limits the method overall accuracy: indeed, those sensors have typically a finite resolution of 5 cm.

Fig. 3 is obtained using the same simple surface defined in Table 1 of [39], where the simulation aims to study the behavior of the Base model when the level of the mass grows, uniformly, within the LDR resolution. Each of these volumes has a base of 20 m × 20 m while the upper surface is uneven and different for each of the volumes.

Obviously, due to the quantization, in Fig. 3 in many cases the Base model returns the same value for the volume with different "true" heights. Nevertheless, when using a low accuracy sensor, the uncertainty of the volume estimation under certain assumptions can be improved using a greater number of sensors, which usually corresponds to a better measurement but also to an increase in the costs of this type of instrumentation that, while not being in general very high, must still be taken into consideration.

In this context, considering the quantization error introduced by the sensor a 0 mean random process, two variants of the Base model described in [39] are presented, with the idea to enhance the volume estimation accuracy. As we will see in the next sections, these models give a better estimation also using analog sensors which do not introduce a quantization error.

The general idea on which the two new models are based is the same for both: place more than one sensor for all or part of the measurement spots. For example, two sensors may be placed symmetrically to the side of the measurement spots, or four sensors may be arranged according to a square layout, with the measurement spot placed exactly in the middle: in this case, the value $a_{i,j}$ which would have been measured in the Base model is replaced with the arithmetic mean of the values returned by the new sensors. The distance between the sensor spots must be such as to have a sufficient probability of being characterized by an independent error. In this perspective, the two proposed models differ only in the choice of the number of sensors to be used on each internal node (2 or 4). These solutions allow for reducing the contribution of the quantization error of an amount which depends on the surface with the upper limit of a factor equal to $1/\sqrt{N}$, where N are the sensors used in each node. A limit to the value of N is set by the node cost, complexity and power consumption, as will be explained in Section 6, therefore we decide to use a maximum of 4 sensors in each node, with the two strategies depicted in Fig. 4.

In particular, the first model, called B2 (Fig. 4(a)), needs:

- a unique sensor at the four corners of the grid;
- two sensors for all remaining nodes.

For this model, the distance between two adjoining measurement spots will be the same of the Base model.

The second model, called B4 (Fig. 4(b)), needs:

- a unique sensor at the four corners of the grid;
- two sensors for each node in the border of the grid;
- four sensors in the internal nodes.

Since this model requires a large number of sensors, to limit such number the measurement spots are placed at a distance which is 1.25 times the one of the B2 model. In any case, it has to be underlined that, despite increasing the number of employed sensors, each configuration foresees the usage of the same number of nodes of the corresponding Base model: indeed, the newly added sensors are simply connected to the already existing nodes.

At this point we show in detail the two new models and later some simulation results. We place ourselves in the same geometric conditions (surface S and square base $l \times l$).

For B2 model, we denote by:

- $a_{0,0}$, $a_{0,n}$, $a_{n,0}$, $a_{n,n}$ the reading values of the sensors placed in the vertices of the base;
- $b^-_{i,j}$, $b^+_{i,j}$ the reading values of the two sensors that replace the sensor that returns the value $a_{i,j}$ in the model in [39], for any sensors but the ones in the corners of the grid.

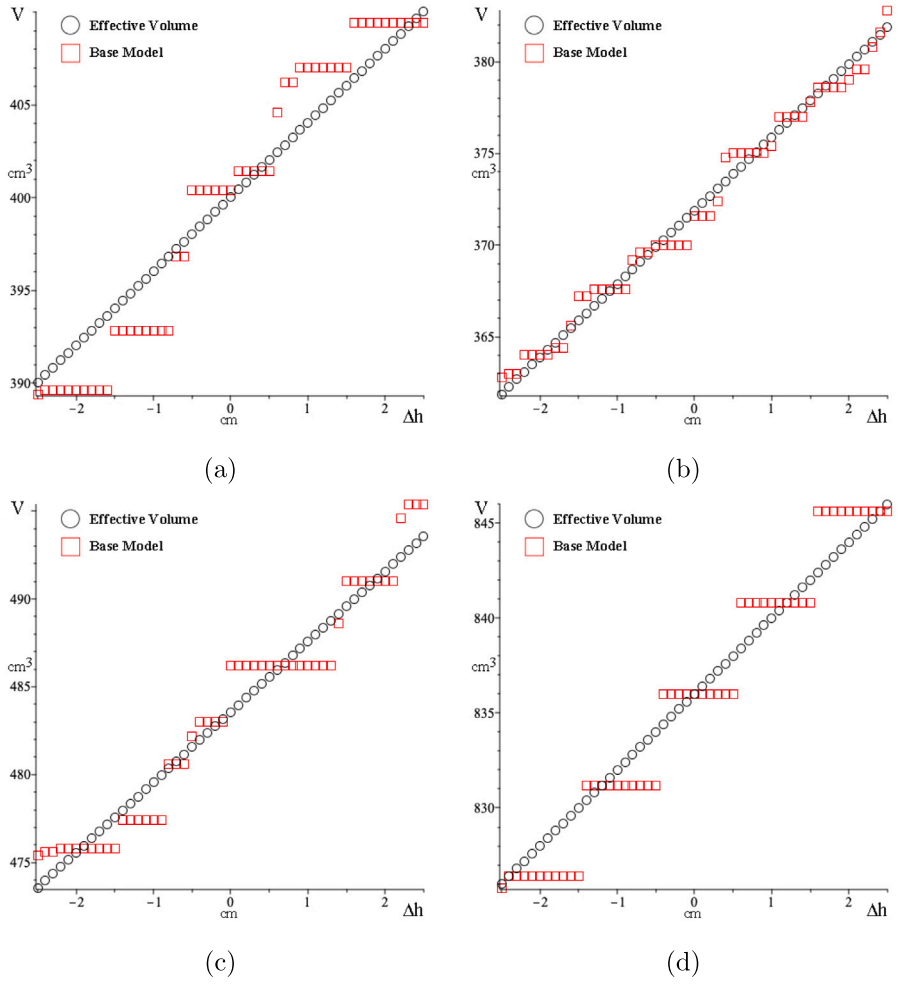

Fig. 3. Simulations using the Base model with surfaces (a), (b), (c) and (d) in [39]. The true volume is defined as $V = \int_a^b \int_c^d (h_i(u,v) + \Delta h) du dv$.

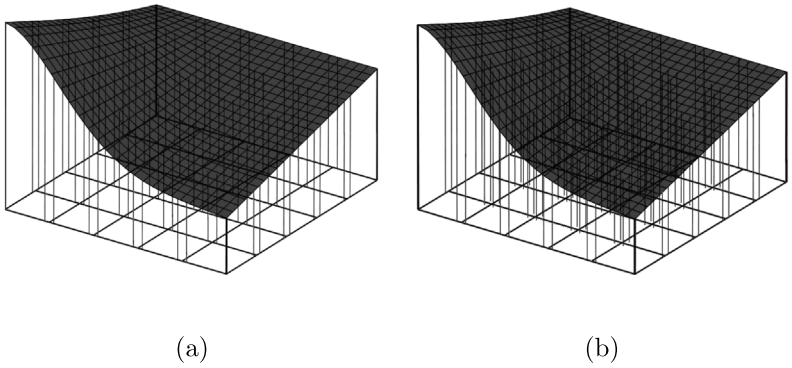

Fig. 4. Sensors disposition for (a) B2 and (b) B4.

This time, the approximate volume obtained is equal to

$$V_{B2} = \frac{l^2}{4n^2} \cdot (a_{0,0} + a_{0,n} + a_{n,0} + a_{n,n}) + \\ + \frac{l^2}{2n^2} \cdot \sum_{i=1}^{n-1} \left(\frac{b^-_{0,i} + b^+_{0,i}}{2} + \frac{b^-_{l,i} + b^+_{l,i}}{2} + \frac{b^-_{i,0} + b^+_{i,0}}{2} + \frac{b^-_{i,l} + b^+_{i,l}}{2} \right) + \\ + \frac{l^2}{n^2} \cdot \sum_{i,j=1}^{n-1} \frac{b^E_{i,j} + b^W_{i,j}}{2}. \quad (3)$$

For B4 model, we denote by:

- $a_{0,0}$, $a_{0,n}$, $a_{n,0}$, $a_{n,n}$ the reading values of the sensors placed in the vertices of the base;
- $b^-_{0,i}$, $b^+_{0,i}$ the reading values of the two sensors that replace the sensor that returns the value $a_{0,i}$ in the model in [39], with $i = 1, \dots, n-1$. Similarly we consider values $b^-_{n,i}$, $b^+_{n,i}$, $b^-_{i,0}$, $b^+_{i,0}$, $b^-_{i,n}$, $b^+_{i,n}$ for the sensors in the other three sides of the base;

- $b_{i,j}^{NE}$, $b_{i,j}^{SE}$, $b_{i,j}^{SW}$, $b_{i,j}^{NW}$ the reading values of the four sensors which replace the internal sensor which returns the value $a_{i,j}$ in the model in [39], with $i, j = 1, \dots, n-1$ (where NE=North-East, SE=South-East, NW=North-West, SW=South-West).

By replacing the averages of the sensors on the sides and in the interior of this model in Equation (2), we obtain that the approximate volume obtained is equal to

$$V_{B4} = \frac{l^2}{4n^2} \cdot (a_{0,0} + a_{0,n} + a_{n,0} + a_{n,n}) + \\ + \frac{l^2}{2n^2} \cdot \sum_{i=1}^{n-1} \left(\frac{b_{0,i}^{-} + b_{0,i}^{+}}{2} + \frac{b_{l,i}^{-} + b_{l,i}^{+}}{2} + \frac{b_{i,0}^{-} + b_{i,0}^{+}}{2} + \frac{b_{i,l}^{-} + b_{i,l}^{+}}{2}\right) + \\ + \frac{l^2}{n^2} \cdot \sum_{i,j=1}^{n-1} \frac{b_{i,j}^{NE} + b_{i,j}^{SE} + b_{i,j}^{SW} + b_{i,j}^{NW}}{4}. \quad (4)$$

With the aim of proving the efficiency of the geometric methods proposed for calculating the volume using sensors with finite resolution, the approximation formulas were tested on the same four different volumes studied in [39] and shown in Fig. 3.

The preliminary simulations aim to study the behavior of the three models when the level of the mass grows, uniformly, from −2.5 cm to 2.5 cm, assuming a quantization of 5 cm in the LDR sensors. In Fig. 5 the black circles represent the linear growth of the true volume. The red squares represent, as before, the corresponding values of volumes computed by the Base model. Finally, the green and blue diamonds represent the corresponding values of volumes computed, respectively, with the B2 model and the B4 model. We can notice that the Base model is not able, in general, to perceive small variations of volume: indeed, for all the four surfaces, looking at the trends it is possible to notice the actual quantization of the volume, with quantization steps which are notably larger than for the other two models. This is much more evident in Figs. 5(c) and 5(d) where the Base model features a limited number of quantization steps: however, here the B2 and B4 models provide a better computation of the volumes due to the shape of the surface which allows, in the simulated environment, for an effective compensation of the quantization error. Indeed, in the case of a single sensor, the error is due only to the quantization error of the sensor itself (i.e., the maximum value is ±2.5 cm). Conversely, when more sensors are positioned in the measurement spot, the actual level is computed as the mean value of the sensors readings. In all the cases when the surface is not flat, sensors positioned close to the same measurement spot may read two different quantization levels. This leads to a mutual compensation of the individual quantization errors.

5. Simulations

A second set of simulations was carried out assuming a configuration close to the actual experimental setup and more in general to real world applications, concerning granular materials forming piles. To this aim, in these simulations a 1 cm sensor resolution was assumed: this value is more in line with the actual accuracy of the ultrasonic sensors used in the final experimental setup. Concerning the material configurations, these were chosen to simulate as much as possible a real scenario of a closed structure housing granular material such as a granary or a warehouse: indeed, in this context the material is generally introduced by means of a central opening or from spots placed close to the outer walls. With such configurations, the material creates a central pile in the first case or an accumulation in the corners or in the sides in the second. Obviously, other configurations may have been chosen. However, the aim of this contribution was to demonstrate the viability of the solution in a general context: for this reason we chose to test the performances on these shapes.

We simulated the granular material pile surface with a 2-D scaled Gaussian with $\sigma_x = \sigma_y$ and maximum $h - h_0$ covering a square area with a side of 150 cm, on top of a parallelepiped with fixed area and base height h_0. We consider also a high spatial frequency harmonic noise to simulate local perturbations and white noise to simulate fine spatial variability due to the granular nature of the material. In any case we pose the physical constraint to the Gaussian slope to be lower than 45°. Note that for the selected surface (A 2-D Gaussian with $\sigma_x = \sigma_y$), the sampling theorem is satisfied when the spatial sampling step is smaller than $\pi * \sigma_x/2$. We therefore, assume a critical value for the Gaussian standard deviation given by $dx/\pi * 2$, being dx the spacing of the sensing nodes, and we assess the algorithm performance for the standard deviations and different noise levels. Very similar results were found until the Gaussian standard deviation remains larger than the critical value, condition which can be easily fulfilled in real cases even with sparse sensors grids. The results presented hereafter are related to a Gaussian with $\sigma = 150$ cm and considering a noise level given by white noise with a standard deviation $0.2 * (h - h_0)$, and harmonic noise with $0.2 * (h - h_0)$ amplitude.

From these results it can be seen that the estimation errors provided by the proposed models are functions of the Gaussian height $(h - h_0)$ relative to the base height (h_0). This is an obvious result, since this parameter measures the non-flatness of the surface and its impact on the volume, having the base a constant area. Moreover, it was found that the worst situation, as far as the error is concerned, is found when the Gaussian peak, the top of the pile, is placed in the center of the square base, as can be seen from the following configurations (shown in Figs. 6(a) to 9(a)):

- Configuration #1, with the vertex of the pile in central spot;
- Configuration #2, with the vertex of the pile the central spot of one of the sides;
- Configuration #3, with the vertex of the pile in one of the corners;
- Configuration #4, with the vertex of the pile placed in a random spot of the monitoring area.

For each configuration, the estimation of the volume was performed on 30 different surfaces, obtained by progressively increasing the value of the height of the pile vertex. The volumes were computed on the same surfaces for each of grid layouts, in order to make the results comparable. Four grid layouts were tested. The Base model was tested assuming two different spatial samplings: a "sparse" configuration with 5 sensors per side (a sensor every 37.5 cm) and a "dense" configuration with 6 sensors per side (a sensor every 30 cm). Then, the B2 model was tested in the "dense" configuration while the B4 model was tested in the "sparse" one, resuming the configurations of the experimental setup. This choice was made to keep limited the overall number of sensors: indeed, with this configuration the overall number of sensors was respectively 25 and 36 for the Base models, 68 sensors for the B2 one and 64 sensors for the B4 one. The choice of these quantities of nodes and sensors will be justified in Section 6.

Figs. 6(b) to 9(b) show the estimation error of the system in function of the pile height and for the four material layout configurations. First of all, it is evident that in all cases the error tends to stabilize around a certain value from a certain height onward. For all the cases, the stabilization value is lower than 7%, which is in general a satisfying performance. Moreover, for 3 cases out of 4 the value drops below 4%, which is in line with the first set simulations. It is also evident that, in general (see Figs. 6(b) and 9(b)), a higher spatial resolution means a lower error. While this aspect was predictable, it is interesting to observe that this difference is not noticeable for configurations #2 and #3 (Figs. 7(b) and 8(b)): this is probably due to the fact that in these cases the pile is configured as an almost linear slope, thus the accuracy of the interpolation does not increase with a larger spatial sampling.

Conversely, the increase in the number of sensors for measurement spot (models B2 and B4) does not seem to provide the positive effect noticed with the preliminary simulations presented in Section 4. While the presence of more sensors improves the accuracy for the layout based on the sensors featuring the 5 cm resolution adopted in Section 4, this does not happen for sensors with higher accuracy like the ones adopted

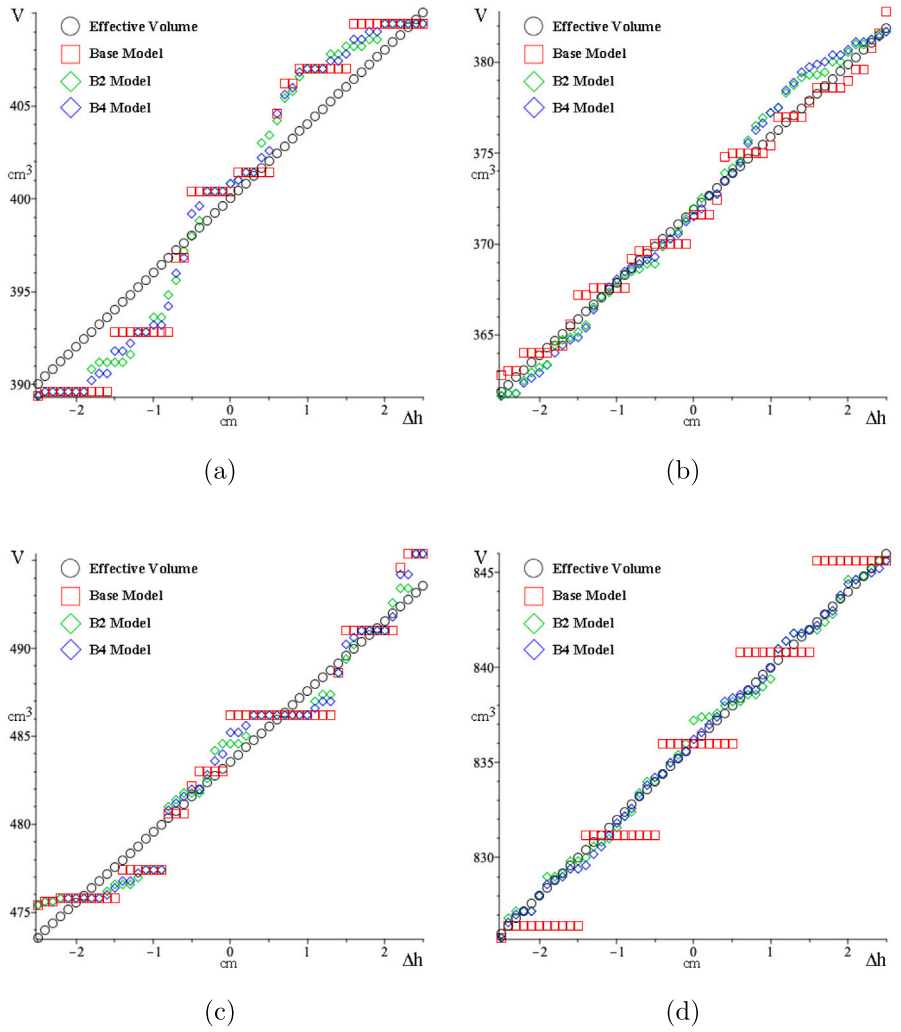

Fig. 5. Simulations using the three models with surfaces (a), (b), (c) and (d) in [39]. The true volume is defined as $V = \int_a^b \int_c^d (h_i(u,v) + \Delta h) du dv$.

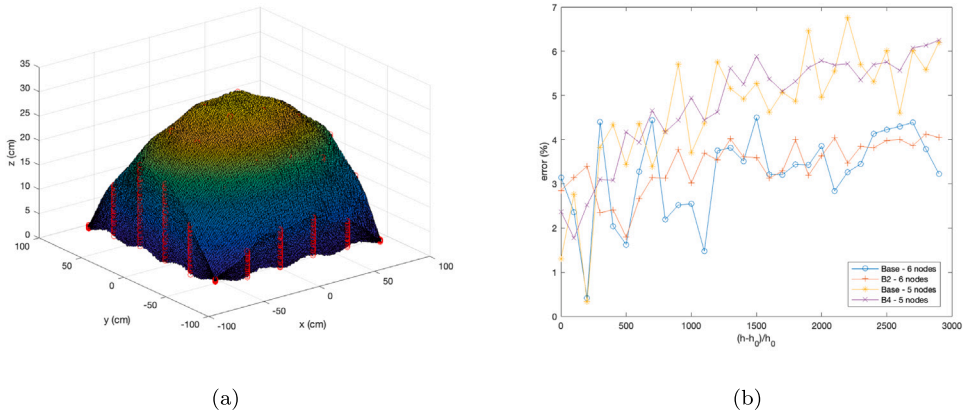

Fig. 6. Configuration #1 - Pile vertex in central position: (a) simulation volumes and (b) volume estimation error for the four topologies.

in this second set of simulations. This probably derives from the fact that the average value obtained by more than one sensor per spot can partially compensate large quantization errors (e.g., 2–2.5 cm errors): conversely, with a larger accuracy, the compensation becomes almost useless. However, two aspects may suggest the usage of layouts like B2 or B4. First of all, the price of sensors with respect to the overall cost of the nodes is almost negligible: this means that adding more than one sensor may add redundancies to the system increasing its reliability without increasing the system cost and complexity. Secondly, the estimation error is more stable with respect to height variations in case of multiple sensors with respect to the Base model. This is mainly due to the fact that, being the noise simulating the spatial variability δ-correlated, its global standard deviation decreases when increasing the overall density of sensors. For these two reasons, system tests were also performed for all the four material layout configurations.

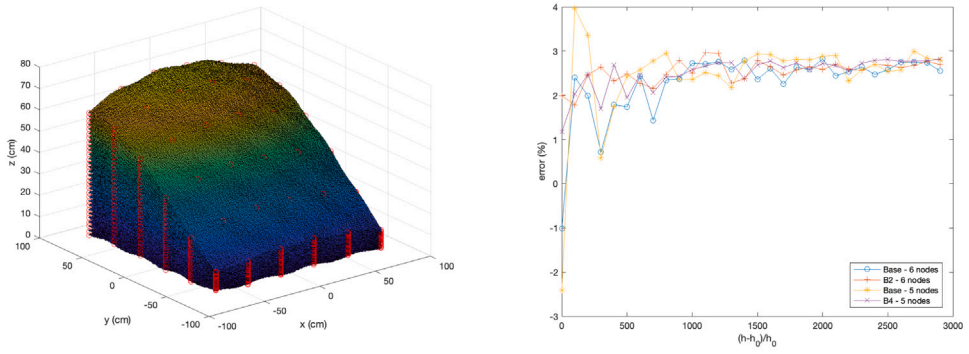

Fig. 7. Configuration #2 - Pile vertex in the middle of one side: (a) simulation volumes and (b) volume estimation error for the four topologies.

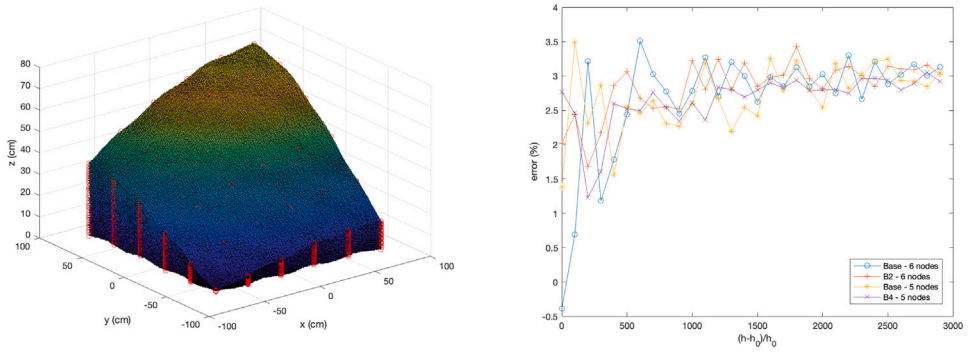

Fig. 8. Configuration #3 - Pile vertex in one corner: (a) simulation volumes and (b) volume estimation error for the four topologies.

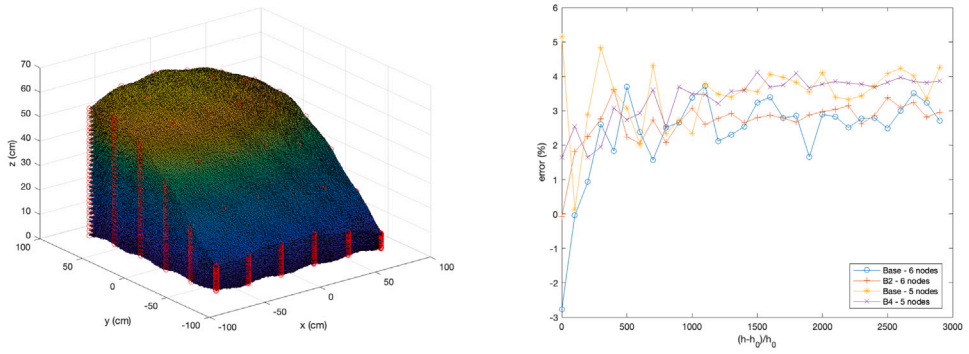

Fig. 9. Configuration #4 - Pile vertex in random position: (a) simulation volumes and (b) volume estimation error for the four topologies.

6. Experimental setup

An ad-hoc experimental setup was implemented in laboratory to test the operation of the system at a reduced scale and under controlled conditions. Such structure foresaw the usage of a metallic grid of 90 cm × 120 cm, below which the sensor nodes were anchored: such grid was then kept at a height of 35 cm by means of 4 wooden poles placed at its vertices (See Fig. 10). The granular material was placed in the volume below the grid: in particular, uniform sand was used for the tests, allowing an accurate calculation of its volume thanks to the almost constant value of its density. The tests were performed using a total of 123.8 kg of sand, featuring a density that was calculated measuring the weight of 1 dm^3 of material by means of a container of known capacity with a scale featuring an accuracy of ±5 g. The calculated density was 1.95 g/cm^3.

Tests were carried out assuming the granular material to be configured as a pile, similarly as the simulations configuration, but setting the level of the material in each point of the perimeter equal to 0. This assumption allowed to enlarge the overall monitored area, while setting up a more critical scenario. Indeed, while the sensors were arranged along a 90 cm × 90 cm square, the overall monitoring area was 150 cm × 150 cm as in the simulations. This configuration implies a larger error since the value in all the points along the measurement perimeter is assumed 0. Indeed, the estimation of the volume of the

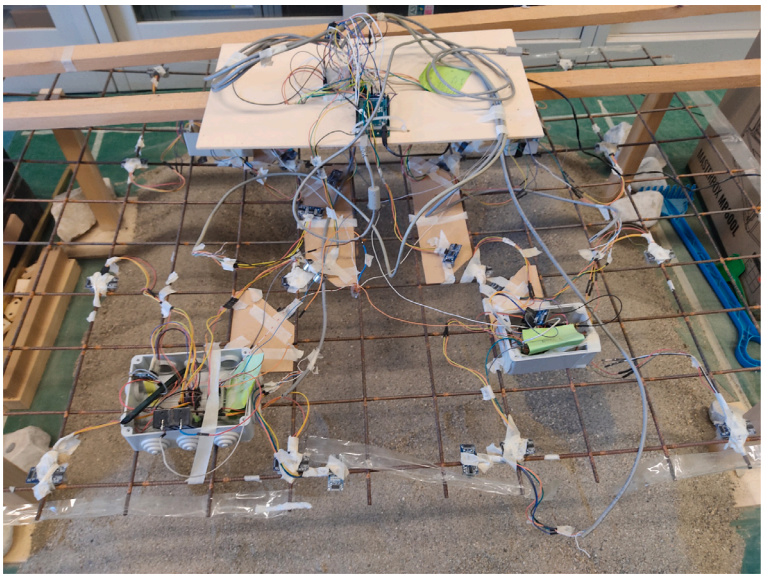

Fig. 10. Experimental setup in laboratory.

material enclosed between the outer nodes and the border (the area between the inner 90 cm × 90 cm square defined by the sensors grid and the overall 150 cm × 150 cm area) implies a larger error.

Together with this aspect, some other assumptions influencing the interpretation of the acquired results have to be made:

- The downsizing of the system has a negative influence on the relative accuracy of the calculated volume. Indeed, the accuracy of the sensors is almost independent from distance, in the sensor measurement range: this means that the relative uncertainty increases when the measured distance is small. For the experimental setup, the measured distance is always lower than 35 cm: since the accuracy of the sensors is ±1 cm (See Section 2), the relative uncertainty for this configuration is higher than 2.5%;
- As already said, if using relative error to assess the volume estimation system performance, the used thin layer of sand brings the system to a worst case working situation, characterized by the limit error value (see the simulation results in the previous section). This must be taken into account when comparing the results with others reported in the literature. For example, the 1% accuracy estimated in [39] was obtained with a layout of 20 m × 20 m, with the sand layer having an average value of at least 1 m.

7. System tests

In order to validate the system as well as the computation technique, 3 different surface shapes were created. As for the case of the simulations, these shapes were chosen to simulate as much as possible real scenarios of a closed structure housing granular material, assuming the case of the central pile presented in Section 5 together with two other significant cases that were easily implementable in the experimental setup. Indeed, the cases with the vertex in the corner and in the middle of one size were not implementable due to the absence of external walls in the setup, as described in Section 6. The tested surface layouts were then the following:

S1: the upper surface is higher in the center and lower in the corners, with a difference of level of about 30 cm and a smooth profile. This is the pile configuration with the central vertex adopted in the simulations;

S2: the upper surface is higher on the borders (Fig. 11(a)) and lower in the center. Such configuration may resemble the case when the material is removed from the center of the warehouse or introduced from the sides;

S3: the upper surface is created randomly in order to resemble a general case where the flatness of the surface is perturbed by noise (Fig. 11(b)).

These shapes were created using two different quantities of sand and thus for two different heights: first, a "*Low Level*" configuration was tested, using only 62 kg of sand, for a total volume of ∼ 31794 cm^3 of sand. Then a "*High Level*" configuration was tested, employing all the 123.8 kg, for a total volume of ∼ 63487 cm^3 of sand.

For each of these shapes, 150 measurements for each sensor were acquired, for each of the grid configurations described in Section 6. As described in Section 6, a square surface featuring the external edges of length l = 150 cm was adopted. Tests were carried out for the four sensor layouts presented in Section 5. For Base (6 nodes) and B2 model, level measurements were acquired at spots separated by a distance of 30 cm, with a total of $6 \cdot 6 = 36$ measurement points (and thus a total number of $n \cdot n = 5 \cdot 5 = 25$, 30 cm × 30 cm sub-squares). For Base (5 nodes) and B4 model, level measurements were acquired at spots separated by a distance of 37.5 cm, with a total of $5 \cdot 5 = 25$ measurement points (and thus a total number of $n \cdot n = 4 \cdot 4 = 16$, 37.5 cm × 37.5 cm sub-squares). In both cases, the values of the external spots were set by default to 0 as explained in Section 6. Despite a different number of measurement spots, for all the models the measurement area was 150 cm × 150 cm = 22 500 cm^2: the measurement capability was thus the same for all the solutions.

As anticipated, the Base model foresaw the presence of only one sensor for each measurement spot: the total number of sensors was thus equal to 9 for the 5 nodes layout (with 16 external points set to 0) and 16 for the 6 nodes layout (with 20 external points set to 0). For model B2 we had 4 single sensors in the corners and 12 couples of sensors in all the other spots, for a total number of 28 sensors with 20 additional points set to 0. For model B4 we had 4 single sensors in the corners, 4 couples of sensors in the intermediate spots on the edges (1 per edge) and 1 group of 4 sensors for the inner spot, again for a total number of 16 sensors plus 16 external points set at 0. The four layouts are shown in Figs. 12 and 13.

Together with these acquisitions, a baseline one was also performed, removing all the sand from the area below the grid. This acquisition was required to remove the biases introduced by the different levels

(a) (b)

Fig. 11. Two different shapes of the upper surface.

of the grid: indeed, due to its weight, the central part of the grid was slightly curved down with respect to the points where the grid was held by the poles. The acquired values, which represented the actual distance of the sensors from the floor were then exploited to calculate the actual thickness of the sand in each specific spot, by subtracting the values which had been acquired during the other measurements to these baseline ones.

In order to acquire all the measurements, five sensor nodes where set up. Four sensor nodes followed exactly the architectural layout described in Section 2 except for the fact that each node was connected to 4 ultrasonic sensors. A last node was set up, to simplify the system, using an Arduino Mega board, which allowed the simultaneous connection of 12 sensors: this node was used only for the tests performed with B2 model.

Since tests were performed in a laboratory, thus without the need for long transmission ranges, LoRaWAN settings were chosen to reduce the timing: for this reason, the chosen settings were SF 7, CR 4/5 and BW 125 kHz. With these parameters, the airtime for a 50 byte packet is 118 ms, which means, taking into account the 1% duty-cycle regulation, a total time of around 30 minutes to transmit 150 packets. However, we would like to point out that the 150 measurements are expected to be pre-processed on node in a real implementation of the system: in this case, only one packet carrying the actual measured value will be transmitted.

Transmitted packets were received by an LG308 LoRaWAN gateway produced by Dragino, embedding two SX1257 LoRa transceivers and one SX1301 LoRa modem, both produced by Semtech. The gateway forwarded the packets to a custom made LoRaWAN server in charge of storing the data inside a MySQL database. Eventually, in the final implementation of the system the volume may be computed directly on the gateway, and then only its value forwarded to the server.

8. Results and discussion

The actual uncertainty for the volume measurement can be computed according to the propagation of uncertainties by resorting to Equations (3) and (4): the values are ± 1123 cm^3 for Base (6 nodes) and B2 models, and ± 1075 cm^3 for Base (5 nodes) and B4 models, with a lower value for Base (5 nodes) and B4 models deriving from the lower number of sensors. However, these values do not take into account the uncertainty deriving from the model error, i.e., the approximation of the integral provided by the sums in Equations (2) to (4). This uncertainty contribution is combined with the model error studied in the previous sections through simulations, which tends to limit values larger than this contribution.

In order to improve the accuracy of the estimated value, data were pre-processed before computing the volume itself. First, we removed outlying values deriving from unpredictable errors (in few cases sensors provided values which were by far larger than their distance to the soil). Then, we considered a sliding window with length 20 observations and we computed the sliding means of the measurements for each sensor, to be used in Equations (3) and (4). For each configuration and for each model, the results are summarized in Tables 1 to 4, where the mean $\overline{V}$ and the standard deviation $\sigma(V)$ of the estimates are reported. To better visualize the behavior of the volume estimation methods, we also reported the relative bias with respect to the true volume TV, defined as $|\overline{V} - TV|/TV$, and the coefficient of variation $CV = \sigma(V)/\overline{V}$.

Table 1
Results of the experiments for the Base (6 nodes) model.

Level	Shape	mean (sd)	Bias(%)	CV(%)
Low level TV = 31794 cm^3	S1	36442 (366) cm^3	14.62%	1.00%
	S2	27169 (828) cm^3	14.55%	3.05%
	S3	32679 (557) cm^3	2.78%	1.69%
High level TV = 63487 cm^3	S1	67849 (293) cm^3	6.87%	0.43%
	S2	68711 (340) cm^3	8.23%	0.49%
	S3	58054 (474) cm^3	8.56%	0.82%

Table 2
Results of the experiments for the B2 model.

Level	Shape	mean (sd)	Bias(%)	CV(%)
Low level TV = 31794 cm^3	S1	33969 (254) cm^3	6.84%	0.75%
	S2	29495 (427) cm^3	7.23%	1.45%
	S3	31826 (298) cm^3	0.10%	0.94%
High level TV = 63487 cm^3	S1	69388 (379) cm^3	9.29%	0.55%
	S2	66057 (269) cm^3	4.05%	0.41%
	S3	61103 (396) cm^3	3.76%	0.65%

Table 3
Results of the experiments for the Base (5 nodes) model.

Level	Shape	mean (sd)	Bias(%)	CV(%)
Low level TV = 31794 cm^3	S1	36382 (773) cm^3	14.43%	2.12%
	S2	26562 (305) cm^3	16.46%	1.15%
	S3	28539 (512) cm^3	10.24%	1.79%
High level TV = 63487 cm^3	S1	87386 (486) cm^3	37.64%	0.56%
	S2	52528 (433) cm^3	17.26%	0.82%
	S3	55365 (279) cm^3	12.79%	0.50%

Table 4
Results of the experiments for the B4 model.

Level	Shape	mean (sd)	Bias(%)	CV(%)
Low level TV = 31794 cm^3	S1	39803 (481) cm^3	25.19%	1.21%
	S2	29008 (308) cm^3	8.76%	1.06%
	S3	35891 (388) cm^3	12.88%	1.08%
High level TV = 63487 cm^3	S1	74956 (2062) cm^3	18.07%	2.75%
	S2	65682 (416) cm^3	3.46%	0.63%
	S3	70430 (294) cm^3	10.94%	0.42%

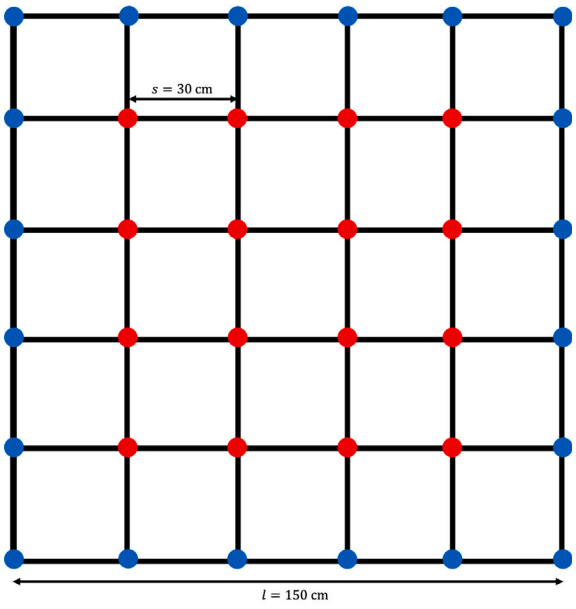

(a)

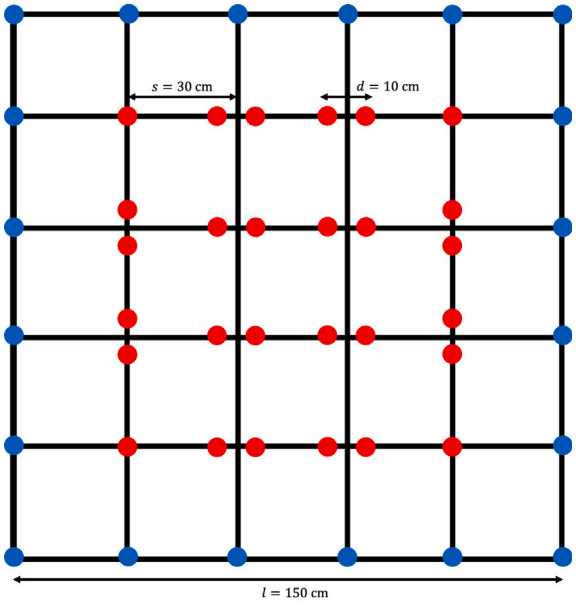

(b)

Fig. 12. Sensors deployment in the experimental layout for (a) Base - 6 points and (b) B2. The red dots indicate the positions of the sensors, the blue dots indicates the spots with value set to 0, l is the overall surface edge length, d is the distance among two measurement spots and s is the distance among two sensors in the spots with multiple sensors.

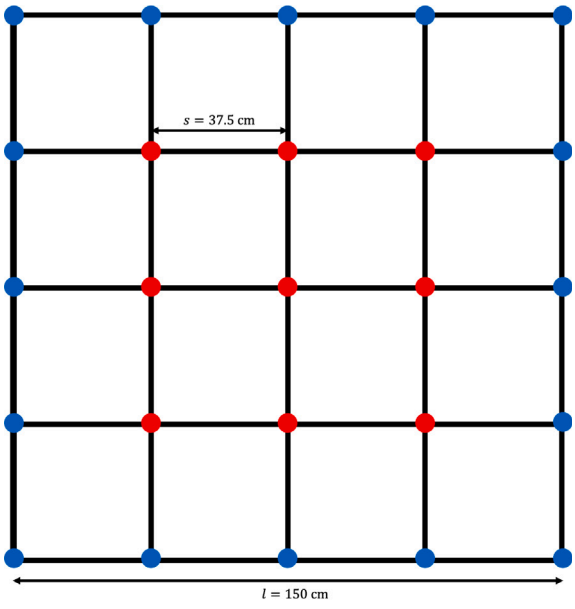

(a)

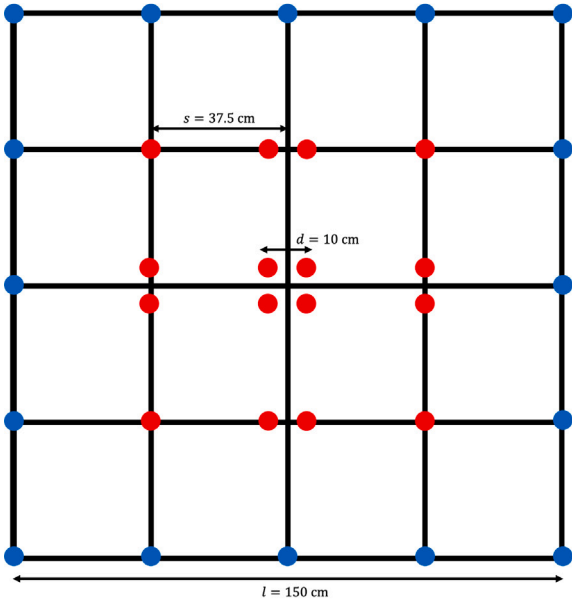

(b)

Fig. 13. Sensors deployment in the experimental layout for (a) Base - 5 points and (b) B4 models. The red dots indicate the positions of the sensors, the blue dots indicates the spots with value set to 0, l is the overall surface edge length, d is the distance among two measurement spots and s is the distance among two sensors in the spots with multiple sensors.

From Tables 1 to 4 we see that:

- as expected, the best results are achieved for B2 model which, in general, overcomes the other configurations both in terms of bias and coefficient of variation;
- it is evident that adding more sensors for each measurement spots increases the accuracy. B2 model outperforms the corresponding Base model (6 nodes) in 5 cases out of 6 for bias and in 5 cases out of 6 for variability while B4 model outperforms the 5 nodes Base model in 4 cases out of 6 for bias and in 5 cases out of 6 for variability;
- in general, performances are improved more by increasing the spatial sampling grows rather than adding more sensors. Indeed, it is evident that the lower spatial sampling (1 node each 37.5 cm) is not sufficient to ensure a bias lower than 10%, and thus an adequate accuracy.

Some results may appear as unexpected. In particular:

- for Base (6 nodes) model, High Level, we achieve the worst performances for the flat random surface;
- for B4 model, we get the best results for S2 surface, while these should be achieved always for the flat random surface.

All these results may be due to the fact that all surfaces are manually created (basically as it happens in a real use-case), thus a certain degree of variation (and then a certain inaccuracy) has to be taken into account. Such limited repeatability is however inherent in the real use case. For this reason, these experimental results should be evaluated together with the simulation results obtained in Sections 4 and 5. Since all simulation results suggest that increasing the number of sensors leads to a larger accuracy in the evaluation of the volume, and that this result is found in most cases also in the experimental tests, we can conclude that B2 and B4 configurations should always be preferred in a real scenario. In all cases, it is evident that the most significant parameter affecting the accuracy of the measurements is the overall measurement spot spatial density, which should be as high as possible.

9. Conclusions

The aim of this paper was to demonstrate the usability of grids of ultrasonic sensors for the estimation of the volume of granular materials: together with the hardware infrastructure, also a mathematical model was developed to calculate the material volume from the sensor readings. Such model has as the main target the reduction of the computational complexity and, as a matter of fact, can be easily implemented on a very simple microcontroller.

To test the proposed approach, a preliminary set of simulations was carried out. Then, an experimental setup was implemented, simulating a closed environment housing a pile of granular material: in this reduced-size setup, the relative uncertainties are obviously larger that in a real case, thus suggesting that the proposed results can be seen as lower bound concerning the system performances.

In such experimental setup, different sensor layouts were tested, suggesting that the sensor disposition highly affects the system performances. The results suggest that a larger spatial sampling notably increases the performances of the system. Similarly, a number of sensors means a slightly larger accuracy: however, the achievable improvement may not be such consistent to justify the extension of the technological infrastructure.

To fully validate the proposed technique, a long term test, for example in a warehouse, should be carried out. However, a number of difficulties make this test extremely complex to be set up. First of all, in a real scenario the actual measurement of the volume, to be compared with the value acquired by the sensor network, is very difficult to be performed due to the large quantity of required material. Secondly, the installation of the sensors below the ceiling of a building is not straightforward and may be justified only in case of a permanent installation. While we hope that we will be able to perform this test in the future, we believe that the proposed results can be however assumed as effective since they are achieved in worst case scenario conditions.

Together with the implementation of the proposed architecture in a real environment, future work will also focus on different layouts for the sensing technique: indeed, while ultrasonic sensor proven to be an effective choice, the system is expected to be tested employing also different sensing strategies like the ones discussed in Section 2. Among the possible architectures, we are planning to focus in particular on pressure sensors to be positioned below the granular material: this choice will allow the use of the proposed solution also in the case of granular material positioned outdoor (i.e., without any coverage). Moreover, work is expected to be carried out to improve the accuracy of the system: to this aim, the identification of hybrid architectures is seen as a promising approach. In this context, the combination of different sensing strategies (e.g., the combined use of ultrasonic sensors and pressure sensors or the usage of level poles for the perimeter points) may increase the accuracy of the level measurements in each spot, with a higher precision in the overall volume estimation. Finally, the accuracy of the volume estimation may also benefit from the implementation of different sensor layouts: this aspect requires investigation by means of simulations before moving to an actual implementation of the system.

CRediT authorship contribution statement

Alessandro Pozzebon: Conceptualization, Methodology, Visualization, Writing – original draft, Writing – review & editing, Resources. **Marco Benini:** Methodology, Formal analysis. **Cristiano Bocci:** Conceptualization, Methodology, Formal analysis, Writing – original draft. **Ada Fort:** Supervision, Formal analysis, Writing – review & editing. **Stefano Parrino:** Investigation, Methodology, Validation. **Fabio Rapallo:** Formal analysis, Visualization, Writing – original draft.

Declaration of competing interest

The authors declare that they have no known competing financial interests or personal relationships that could have appeared to influence the work reported in this paper.

Data availability

Data will be made available on request

References

[1] R.M. Nedderman, Statics and Kinematics of Granular Materials, Cambridge University Press, 2005.
[2] P. Richard, M. Nicodemi, R. Delannay, P. Ribiere, D. Bideau, Slow relaxation and compaction of granular systems, Nat. Mater. 4 (2) (2005) 121–128.
[3] S. Cuniolo, I. De Lotto, A. Scianna, A stereo vision system for volume measurements, in: Fifth International Conference on Image Processing and its Applications, 1995, pp. 702–706.
[4] J. Li, G. Liu, Y. Liu, A dynamic volume measurement system with structured light vision, in: 2016 31st Youth Academic Annual Conference of Chinese Association of Automation, YAC, 2016, pp. 251–255.
[5] P. Artaso, G. Lopez-Nicolas, Volume estimation of merchandise using multiple range cameras, Measurement 89 (2016) 223–238.
[6] I. Nyalala, C. Okinda, L. Nyalala, N. Makange, Q. Chao, L. Chao, K. Yousaf, K. Chen, Tomato volume and mass estimation using computer vision and machine learning algorithms: Cherry tomato model, J. Food Eng. 263 (2019) 288–298.
[7] T. Apicella, G. Slavic, E. Ragusa, P. Gastaldo, L. Marcenaro, Container localisation and mass estimation with an RGB-D camera, in: ICASSP 2022-2022 IEEE International Conference on Acoustics, Speech and Signal Processing, ICASSP, 2022, pp. 9152–9155.
[8] J.T. Wang, Z.Y. Liu, L. Zhang, L.G. Guo, X.S. Bao, L. Tong, Automatic measurement system for vertical tank volume by electro-optical distance-ranging method, Appl. Mech. Mater. 26 (2010) 416–421.
[9] Q. Xu, Y. Huang, L. Xing, Z. Tian, Z. Fei, L. Zheng, A fast method to measure the volume of a large cavity, IEEE Access 3 (2015) 1555–1561.
[10] A. Irvem, Application of GIS to determine storage volume and surface area of reservoirs: The case study of Buyuk Karacay dam, Int. J. Eng., Technol. Nat. Sci. 1 (2011) 39–43.
[11] S. Lu, N. Ouyang, B. Wu, Y. Wei, Z. Tesemma, Lake water volume calculation with time series remote-sensing images, Int. J. Remote Sens. 34 (22) (2013) 7962–7973.
[12] A.K. Sahoo, S.K. Udgata, A novel ANN-based adaptive ultrasonic measurement system for accurate water level monitoring, IEEE Trans. Instrum. Meas. 69 (6) (2019) 3359–3369.
[13] C.A. Diaz, A. Leal-Junior, C. Marques, A. Frizera, M.J. Pontes, P.F. Antunes, S.B. André, M.R. Ribeiro, Optical fiber sensing for sub-millimeter liquid-level monitoring: A review, IEEE Sens. J. 19 (17) (2019) 7179–7191.
[14] S. Malik, L. Somappa, M. Ahmad, S. Sonkusale, M.S. Baghini, A fringing field based screen-printed flexible capacitive moisture and water level sensor, in: 2020 IEEE International Conference on Flexible and Printable Sensors and Systems, FLEPS, 2020, pp. 1–4.
[15] S. Wang, Y. Yang, L. Zhang, L. Mohanty, R.B. Jin, S. Wu, P. Lu, High-precision fiber optic liquid level sensor based on fast Fourier amplitude demodulation in a specific range of spectrum, Measurement 187 (2022) 110326.
[16] D.K. Fisher, R. Sui, An inexpensive open-source ultrasonic sensing system for monitoring liquid levels, Agric. Eng. Int.: CIGR J. 15 (4) (2013) 328–334.
[17] K. Loizou, E. Koutroulis, D. Zalikas, G. Liontas, A low-cost capacitive sensor for water level monitoring in large-scale storage tanks, in: 2015 IEEE international conference on industrial technology, ICIT, 2015, 2015, pp. 1416–1421.
[18] J.B. Rosolem, D.C. Dini, R.S. Penze, C. Floridia, A.A. Leonardi, M.D. Loichate, A.S. Durelli, Fiber optic bending sensor for water level monitoring: Development and field test: A review, IEEE Sens. J. 13 (11) (2013) 4113–4120.
[19] I.H. Kim, D.W. Lim, J.W. Jung, Single-camera-based sand volume estimation of an excavator bucket, Multimedia Tools Appl. 78 (2019) 5493–5522.

[20] G. Tucci, A. Gebbia, A. Conti, L. Fiorini, C. Lubello, Monitoring and computation of the volumes of stockpiles of bulk material by means of UAV photogrammetric surveying, Remote Sens. 11 (12) (2019) 1471.
[21] J.I. Pagán, L. Bañón, I. López, C. Bañón, L. Aragonés, Monitoring the dune-beach system of guardamar del segura (Spain) using UAV, SfM and GIS techniques, Sci. Total Environ. 687 (2019) 1034–1045.
[22] C.C. de Sousa Mello, D.H.C. Salim, G.F. Simes, UAV-based landfill operation monitoring: A year of volume and topographic measurements, Waste Manag. 137 (2022) 253–263.
[23] A. Pozzebon, I. Cappelli, A. Mecocci, D. Bertoni, G. Sarti, F. Alquini, A wireless sensor network for the real-time remote measurement of Aeolian sand transport on sandy beaches and dunes, Sensors 18 (3) (2018) 820.
[24] M. Vogt, M. Gerding, Silo and tank vision: Applications, challenges, and technical solutions for radar measurement of liquids and bulk solids in tanks and silos, IEEE Microwave Mag. 18 (6) (2017) 38–51.
[25] H. Isiker, H. Canbolat, Concept for a novel grain level measurement method in silos, Comput. Electron. Agric. 65 (2) (2009) 258–267.
[26] E. Yigit, A novel compressed sensing based quantity measurement method for grain silos, Comput. Electron. Agric. 145 (2018) 179–186.
[27] E. Yigit, Development of an expression for the volume of off-centered conical pile inside a cylindrical silo, Measurement 146 (2019) 903–911.
[28] H. Duysak, E. Yigit, Machine learning based quantity measurement method for grain silos, Measurement 152 (2020) 107279.
[29] H. He, X. Xu, T. Chen, P. Lu, Volume measurement of sand carrier using uav-based mapping, ISPRS Ann. Photogramm., Remote Sens. Spatial Inf. Sci. 3 (2020) 19–24.
[30] B.M. Schmid, D.L. Williams, C.S. Chong, M.D. Kenney, J.B. Dickey, P. Ashley, Use of digital photogrammetry and LiDAR techniques to quantify time-series dune volume estimates of the Keeler Dunes complex, Owens Valley, California, Aeolian Res. 54 (2022) 100764.
[31] R.C. Carvalho, R. Reef, Quantification of coastal change and preliminary sediment budget calculation using SfM photogrammetry and archival aerial imagery, Geosciences 12 (10) (2022) 357.
[32] G. Vacca, UAV photogrammetry for volume calculations. A case study of an open sand quarry, in: Computational Science and Its Applications–ICCSA 2022 Workshops, 2022, pp. 505–518.
[33] A.P. Turner, J.J. Jackson, N.K. Koeninger, S.G. McNeill, M.D. Montross, M.E. Casada, M.J. Boac, R. Bhadra, R.G. Maghirang, S.A. Thompson, Stored grain volume measurement using a low density point cloud, Appl. Eng. Agric. 33 (1) (2017) 105–112.
[34] M. Rackl, F.E. Grötsch, M. Rusch, J. Fottner, Qualitative and quantitative assessment of 3D-scanned bulk solid heap data, Powder Technol. 321 (2017) 105–118.
[35] C. Altuntas, Pile volume measurement by range imaging camera in indoor environment, Int. Arch. Photogramm., Remote Sens. Spatial Inf. Sci. 40 (5) (2014) 35.
[36] S. Ding, X. Zhang, Q. Yu, L. Li, J. Wang, A volume measurement method for lunar soil collection based on a single monitoring camera, Sensors 18 (10) (2018) 3394.
[37] L. Yanling, Q. Jian, X. Ning, Study for measurement method for coal volume on base of GPU, in: 2010 2nd International Conference on Future Computer and Communication, 2010, pp. V3–412.
[38] O. Sonbul, P. Popejoy, A.N. Kalashnikov, Ultrasonic sensor array for remote sensing of profiles of bulk materials, in: 2012 IEEE International Instrumentation and Measurement Technology, 2012, pp. 1794–1797.
[39] C. Bocci, A. Fort, A. Pozzebon, D. Bertoni, A geometrical approach for the measurement of the volume of masses of granular material through grid-layout sensor networks, Measurement 151 (2020) 107102.
[40] Microchip, M70/70 bluetooth low energy (BLE) module data sheet, 2023, Avaliable on line: http://ww1.microchip.com/downloads/en/DeviceDoc/BM70-71-Bluetooth-Low-Energy-BLE-Module-Data-Sheet-DS60001372H.pdf. (Accessed on 28 March 2023).
[41] Semtech, SX1272/3/6/7/8 LoRa modem design guide, 2013.
[42] K. Staniec, M. Kowal, LoRa performance under variable interference and heavy-multipath conditions, Wireless Commun. Mob. Comput. (2018).
[43] J. Haxhibeqiri, A. Shahid, M. Saelens, J. Bauwens, B. Jooris, E. De Poorter, J. Hoebeke, Sub-gigahertz inter-technology interference. How harmful is it for LoRa? in: 2018 IEEE international smart cities conference, ISC2, 2018, pp. 1–7.
[44] D. Tamang, A. Pozzebon, L. Parri, A. Fort, A. Abrardo, Designing a reliable and low-latency LoRaWAN solution for environmental monitoring in factories at major accident risk, Sensors 22 (6) (2022) 2372.
[45] LoRa Alliance Technical Committee Regional Parameters Workgroup, LoRaWAN 1.1 Regional Parameters, LoRa Alliance, 2018.
[46] Atmel, Attiny861a data sheet, 2023, Avaliable on line: https://ww1.microchip.com/downloads/en/DeviceDoc/doc8197.pdf (Accessed on 28 March 2023).